Capacity Evaluation of MDOF Systems Subjected To Near-Fault Ground Motion Pulse

A Dissertation Submitted in Partial Fulfillment of the Requirements
for the Master Degree in

Earthquake Engineering

By

Chethan Gouder

Supervisor: Prof.A.Papageorgiou

April, 2008

Istituto Universitario di Studi Superiori di Pavia
Università degli Studi di Pavia

The dissertation entitled "Capacity Evaluation of MDOF Systems Subjected to Near-Fault Ground Motion Pulse", by Chethan Gouder, has been approved in partial fulfillment of the requirements for the Master Degree in Earthquake Engineering.

Prof. A. Papageorgiou_____

ABSTRACT

This study aims at investigating the applicability of an improved ATC-40 Procedure-A suggested by Chopra and Geol to structural systems subjected to a set of near-fault ground motion pulse. The improved ATC-40 Procedure-A is also known as capacity spectrum method, which is a nonlinear analysis technique to evaluate the capacity of structural systems. For this purpose, constant ductility design spectra proposed by Papageorgiou and Mavroeidis for regions having near-fault effect are used to generate demand diagrams which are plots of spectral acceleration vs. maximum displacement. The structural systems used are SAC Three Storey Pre-Northridge buildings designed for three different regions; Los Angeles, Seattle and Boston. Capacity curves are obtained for three different structural systems. P-Delta effects have been included in the analysis.

The capacity of all structural systems for different earthquakes is obtained as the point of intersection of the capacity diagram and demand diagram. The results obtained from capacity spectrum method are compared with time history analysis results. The input for time history analysis are a set of near-fault ground motion pulses generated using the mathematical model suggested by Papageorgiou and Mavroeidis.

The comparison of results obtained from capacity spectrum method and those obtained from time history analysis revealed that the capacity spectrum method gives good results in most of the cases except a few .The discrepancies in results obtained exist due to the impulsive nature of near-fault ground motion.

Keywords: Capacity Spectrum method; Near-fault ground motion; Ground motion pulse

TABLE OF CONTENTS

LIST OF FIGURES

LIST OF TABLES

LIST OF SYMBOLS

Δ_y =Yield Displacement

Δ_u = Ultimate Displacement

f_y =Yield Force

f_u =Ultimate Displacement

K =Pre-yield Stiffness

K_{eff} =Effective Stiffness

T_{eff} =Effective Period

ζ_{eff} =Effective Damping

α =Ratio of Post-yield to Pre-yield stiffness

μ =Ductility

ω_n =Natural frequency

ω =Frequency of excitation

T_p =Pulse Period

ω_p =Frequency of the pulse

M_1^* =Effective Modal mass for first mode

$\mathbf{M}$ =Mass matrix

$\mathbf{C}$ =Damping Matrix

$\mathbf{K}$ =Stiffness Matrix

$\boldsymbol{\phi}$ =Modal Matrix

$\boldsymbol{\phi}_n$ =N-th natural vibration mode

Γ_n =Participation factor of the n-th mode

1 Nonlinear Static Procedures

1.1 Introduction

Nonlinear static procedures are a kind of inelastic analysis which is used to estimate the response of structures to seismic ground shaking. The objective of inelastic seismic analysis procedures is to directly estimate the magnitude of inelastic deformations and distortions. In non-linear static procedures, detailed structural models are simplified into single degree of freedom (SDOF) oscillator models. The ground motion is characterized by response spectra which is a plot of maximum response of a SDOF oscillator as a function of period. Thus the nonlinear static procedure is an approximate procedure with respect to the use of SDOF oscillator over a detailed structural model and also regarding the use of response spectra instead of a detailed ground motion record. Approximations of structural response with an acceptable level of accuracy are what practicing engineers need. This procedure can therefore be used by practicing engineers for seismic evaluation a design upgrades of existing structures and also for design and evaluation of a new construction. The practical objective of inelastic seismic analysis procedures is to predict the expected behavior of the structure in future earthquake shaking. The prediction of the expected behavior of the structure is much needed in performance based engineering (PBE), which uses these predictions to make decisions regarding safety and risk.

1.2 Objectives and Scope

In this study an attempt has been made to evaluate the capacity of SAC Three storey buildings subjected to a set of near-fault ground motion pulses using improved ATC-40 Procedure-A suggested by Chopra and Goel 1999. Constant ductility acceleration and displacement response spectra are used to generate constant ductility demand diagrams instead of demand diagrams based on elastic acceleration and displacement response spectra with different damping, in which inelasticity is indirectly considered using relationships between ductility and damping of equivalent elastic structure. The constant ductility design spectra used in this study are those proposed by Papageorgiou and Mavroeidis 2004 for near-fault ground motion records. P-Delta effects have also been considered. The results of nonlinear static procedure are compared with Dynamic time history analysis results of the same structural systems subjected to near-fault ground pulses proposed by Papageorgiou and Mavroeidis 2003.Only displacement demands have been determined and checked.

1.3 Present Nonlinear techniques

The present nonlinear techniques make use of two methods. The first being equivalent linearization method that is based on the assumption that the maximum displacement of a SDOF oscillator can be estimated by the elastic response of an oscillator with a larger period and damping than that of the actual system. The total displacement comprises of elastic as well as inelastic displacement .The larger damping of the equivalent linear structure is a sum of the actual pre-yield damping of the structure and the damping equivalent to the energy dissipated by hysteresis. The second method is called The Coefficient Method which is fundamentally a displacement modification procedure that is presented in FEMA 356.Displacement modification procedures estimate the total maximum displacement of the oscillator by multiplying the elastic response, assuming initial linear properties and damping by one or more coefficients. The coefficients are typically derived empirically from series of nonlinear response history analysis of oscillators with varying periods and strengths.

1.4 Equivalent linear system

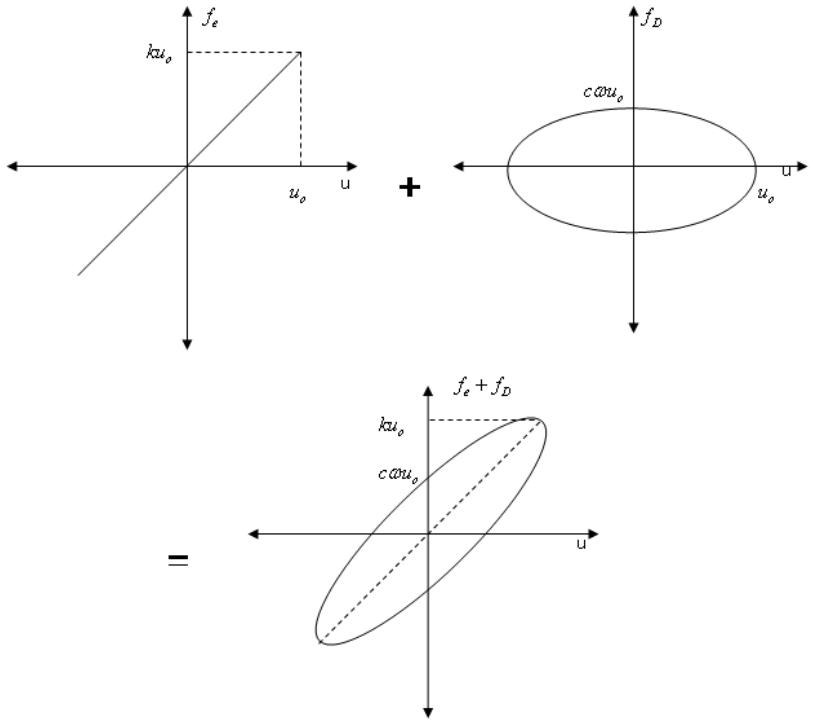

Figure 1-1 Representation of resisting force

The force deformation relationship of any linear SDOF can be described using figure 1.1. The resisting force, which is the force measured during any excitation consists of two components ; force due to damping and the other due to elastic force or the force due to the stiffness of the structure . The total response of the two resisting forces is the inclined ellipse .The energy

dissipated in each cycle is given by the area under the inclined ellipse. The ATC-40 procedures which use the equivalent linear system technique make use of a bilinear force deformation model (figure1.2) with strain hardening.

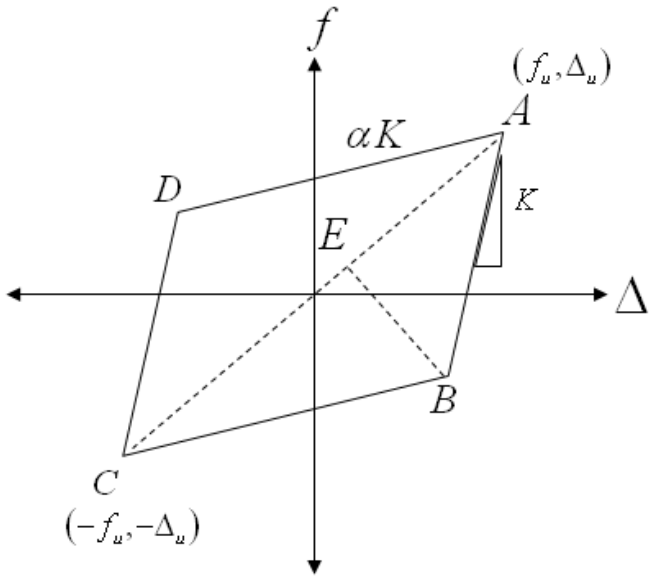

Figure 1-2 Bilinear force Deformation model

1.4.1 Effective stiffness as defined by ATC-40 Procedures

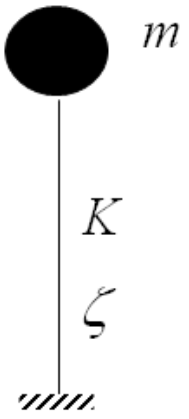

Figure 1-3 SDOF oscillator

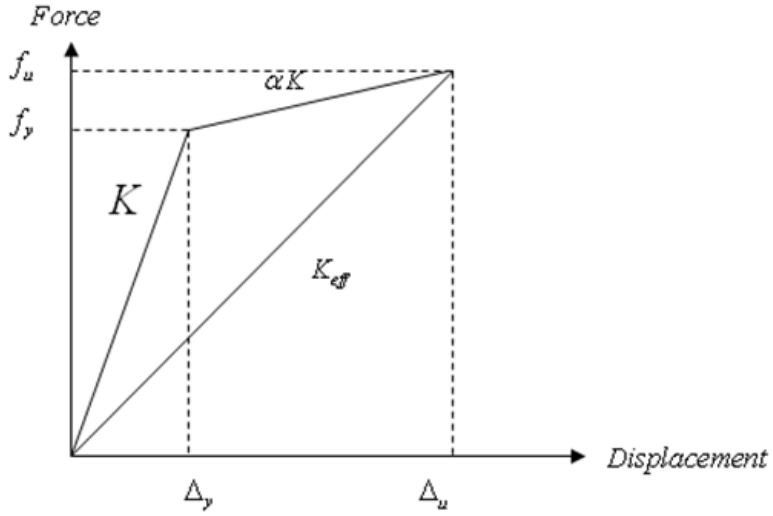

Figure 1-4 Effective Stiffness

From figure 1.4 we can write

$$K_{eff} = \frac{f_u}{\Delta_u}$$

$$K = \frac{f_y}{\Delta_y}$$

$$\alpha K = \frac{f_u - f_y}{\Delta_u - \Delta_y} = \frac{K_{eff}\Delta_u - K\Delta_y}{\Delta_u - \Delta_y} = \frac{K_{eff}\dfrac{\Delta_u}{\Delta_y} - K}{\dfrac{\Delta_u}{\Delta_y} - 1} = \frac{K_{eff}\mu - K}{\mu - 1}$$

$$\therefore\ \alpha K(\mu - 1) = K_{eff}\mu - K$$

$$\Rightarrow \qquad K_{eff} = K\frac{(1 + \alpha\mu - \alpha)}{\mu} \tag{1.1}$$

1.4.2 Effective Period as defined by ATC-40 Procedures

Dividing equation (1.1) by the mass of the system

$$\frac{K_{eff}}{m} = \frac{K}{m}\frac{(1 + \alpha\mu - \alpha)}{\mu}$$

$$\omega_{eff}^2 = \omega^2\frac{(1 + \alpha\mu - \alpha)}{\mu}$$

This gives

$$T_{eff} = T\sqrt{\frac{\mu}{1+\alpha\mu-\alpha}} \tag{1.2}$$

1.4.3 Equivalent Damping as defined by ATC-40 Procedures

Equivalent viscous damping is defined as the energy dissipated by the system when it is excited by a harmonic force with an exciting frequency equal to the natural frequency of the structure.It is also defined as that value of damping which gives the same band width in the frequency response curve as that obtained experimentally for the actual system .Here the former definition is used to determine equivalent damping

The energy dissipated in one cycle, by the system in figure 1. 3 is given by

$$w_D = 2\pi\zeta\frac{\omega}{\omega_n}ku_o^{\,2}$$

Where ω is the frequency of the exciting force.

As stated above, equivalent damping is defined as the energy dissipated by a structure when it is excited by a harmonic force with an exciting frequency equal to the natural frequency of the structure. Therefore

$\omega = \omega_n$

$$\therefore w_D = 2\pi\zeta_{eff}ku_o^{\,2} \tag{1.3}$$

Equation (1.3) can be rewritten as follows

$$w_D = 2\pi\zeta_{eff}ku_o^{\,2} = 2\pi\zeta_{eff}\cdot 2\cdot\frac{1}{2}ku_o^{\,2} = 4\pi\zeta_{eff}E_s$$

$$\therefore \zeta_{eff} = \frac{w_D}{4\pi E_s}$$

Thus the total effective damping can be expressed as

$$\zeta_{Total} = \zeta + \zeta_{eff}$$

The area enclosed by the inclined ellipse of figure 1.1 is equal to w_D . Now if this ellipse is replaced by ABCD of figure 1.2 then

$$w_D = \frac{4\Delta_u^{\,2}\left(\frac{K}{\mu}\right)^2(1-\mu)(1-\alpha)}{K}$$

Therefore we can write

$$\therefore \zeta_{eff} = \frac{1}{4\pi} \frac{4\Delta_u{}^2 \left(\frac{K}{\mu}\right)^2 (1-\mu)(1-\alpha)}{\frac{1}{2}\frac{K[1+\alpha\mu-\alpha]}{\mu}} = \frac{2(1-\mu)(1-\alpha)}{\pi\mu[1+\alpha\mu-\alpha]}$$

This gives us the equation given in ATC-40 for effective damping.

The above derivations indicate that the whole equivalent stiffness technique used in ATC-40 Procedure A is based on the bilinear model ABCD. Effective damping is usually multiplied with a modification factor to take into consideration the various hysteretic behaviors of the structural systems. Reduction factors are defined for constant acceleration and constant velocity regions of the linear elastic design spectrum based on equivalent damping. Thus this method consists of an analysis of a set of equivalent linear SDOF systems using capacity curve and demand diagrams.

1.5 ATC-40 Capacity spectrum method

1.5.1 Procedure

A brief summary of the ATC-40 Capacity spectrum method

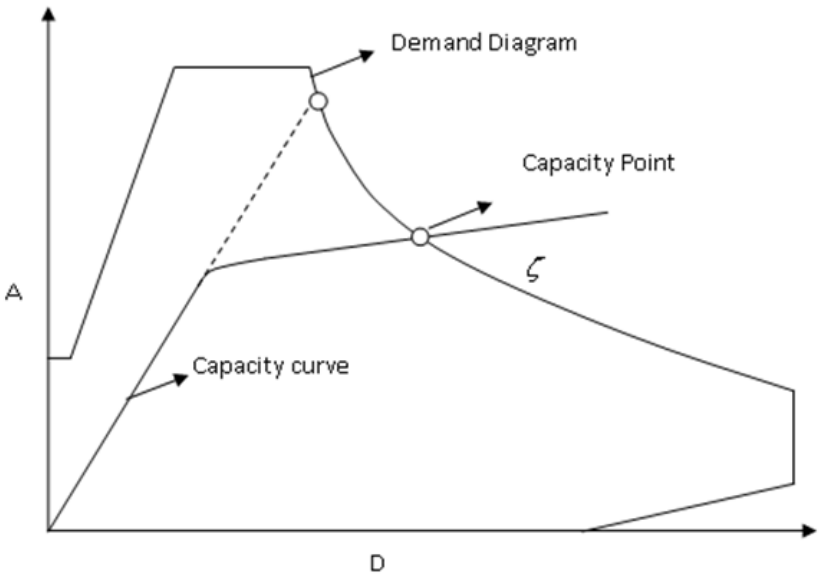

Figure 1-5 ATC-40 Procedure A

1. Obtain the pushover curve
2. Convert the pushover curve to capacity diagram
3. Convert the elastic response spectrum from the standard pseudo-acceleration, *A*, versus natural period, T_n , format to the *A*-*D* format, where *D* is the deformation spectrum ordinate

4. Plot the demand diagram and capacity diagram together and determine the displacement demand .Iterations are made so that the equivalent damping calculated using the ductility value obtained at the point of intersection with the demand diagram matches with the damping value for which the curve is generated.
5. Convert the displacement demand determined in the previous step to global (roof) displacement and individual component deformation and compare them to the limiting values for the specified performance goals.

1.5.2 Drawbacks of the ATC-40 Capacity spectrum method Procedure –A

It has been concluded by Chopra and Goel 2000 that the ATC-40 Procedure does not converge in some cases. They have also concluded that even though if the ATC-40 method converges, the deformation values do not match with the RHA of the inelastic system in many cases.

1.6 Improved ATC-40 Procedure-A

Since studies reveal that the ATC-40 Procedure-A does not give good results, an improved procedure has been used, which makes use of constant ductility design spectra. This is a direct procedure in which the ductility calculated at the intersection of capacity curve and demand diagram known as the capacity point, is compared with the ductility value for which the corresponding demand diagram is generated.

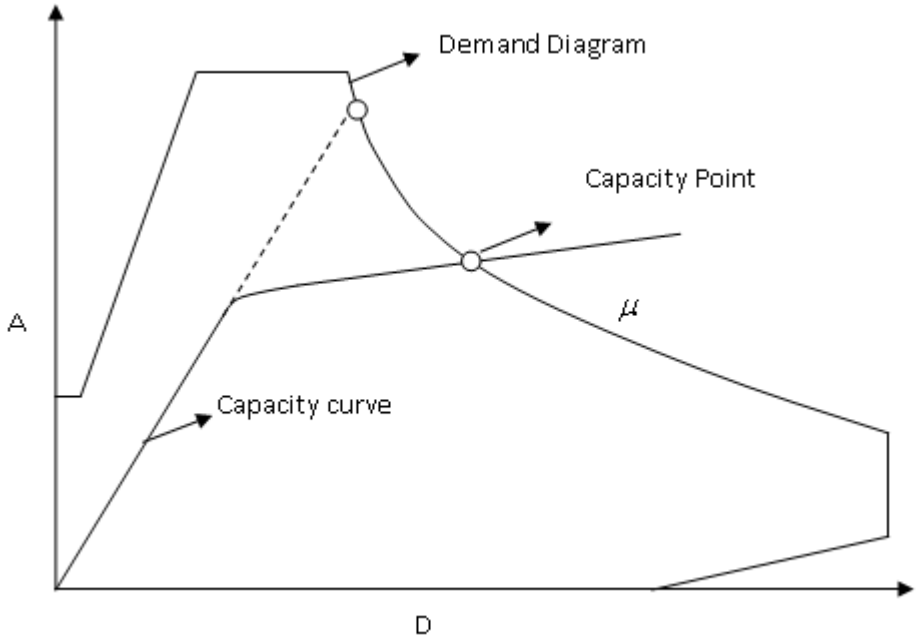

Figure 1-6 Improved ATC-40 Procedure A

A brief summary of the improved ATC-40 procedure A

1. Obtain the pushover curve

2. Convert the pushover curve to capacity diagram
3. Convert the Constant ductility response spectrum from the standard pseudo-acceleration, *A*, versus natural period, T_n , format to the *A-D* format, where *D* is the maximum deformation got by multiplying the constant ductility displacement spectrum ordinate with the ductility of the curve..
4. Plot the demand diagram and capacity diagram together and determine the displacement demand .Iterations are made so that the ductility calculated at the capacity point matches with the ductility of the corresponding demand diagram.
5. Convert the displacement demand determined in the previous step to global (roof) displacement and individual component deformation and compare them to the limiting values for the specified performance goals.

1.7 Outline for report

In Chapter 2 a detailed discussion about the generation of demand diagrams has been made.
In Chapter 3 equations representing the ground motion pulse have been presented.
In Chapter 4 Theoretical background behind the capacity curve has been discussed.
In Chapter 5 Details about the structural models used in analysis have been discussed.
In Chapter 6 results of analysis and conclusions have been presented.

2 Generation of Demand Diagram

2.1 Introduction

To estimate seismic deformations an improved method (Chopra and Goel 2000) has been used. This procedure is similar to ATC-40 Procedure A; Capacity Spectrum Method (CSM). The only difference is the use of constant ductility demand diagrams or constant ductility acceleration maximum displacement response spectrum (AMDRS) instead of elastic acceleration displacement response spectrum (ADRS) reduced for equivalent damping as in ATC-40 Procedure A. In order to implement this improved procedure for structures subjected to near fault ground motion, we have to generate constant ductility demand diagrams using design spectra suggested for regions having near fault effect. For this purpose idealized velocity response spectrum proposed by Papageorgiou et.al. 2004 for near fault ground motion have been used. In the following sections, a detailed description of the procedure used to generate the demand diagrams is discussed

2.2 Design Spectrum

The proposed idealized design spectrum used to generate demand diagrams is for near fault ground motion. It is a four way logarithmic plot with normalized velocity and period axis .The Pseudo-velocity (PSV) axis is normalized by Peak Ground Velocity (PGV) and the period axis by T_p which is the pulse duration. The idealized design spectrum is shown in Figure 2.1

2.2.1 Equations used for generating elastic design spectra

Inelastic response spectrum quantities proposed by Newmark and Veletsos are used

$$SD_y = Yield\ deformation\ ,\ PSV_y = Pseudo\ Velocity = \left(\frac{2\pi}{T_n}\right) SD_y = \omega_n SD_y$$

$$PSA_y = Pseudo\ \ Acceleration = \left(\frac{2\pi}{T_n}\right)^2 SD_y = \omega_n^2 SD_y$$

The above equations can be combined and written as

$$PSV_y = \omega_n SD_y = \frac{PSA_y}{\omega_n} \tag{2.1}$$

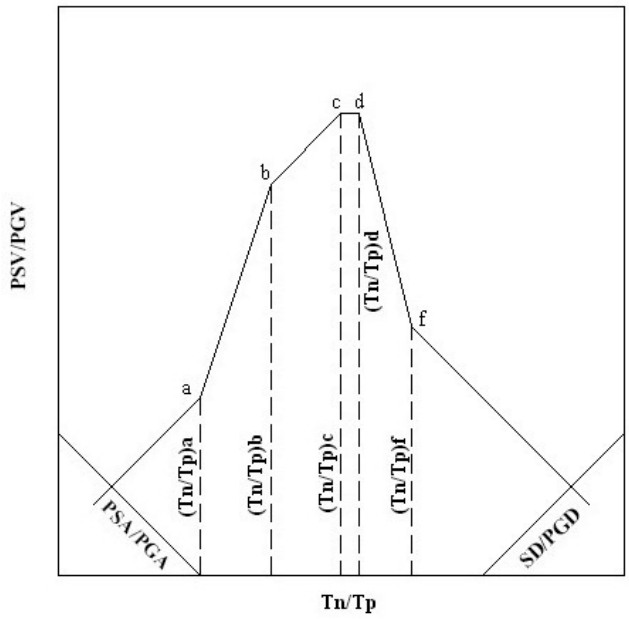

Figure 2-1 Idealized Response Spectrum

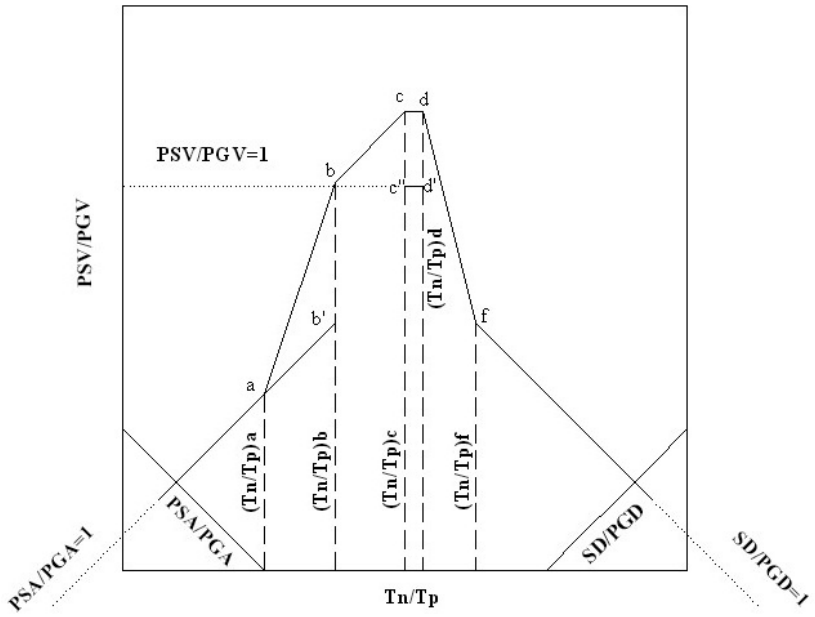

Figure 2-2 Various Stages in the construction of Idealized Velocity Response Spectra

To check the displacement estimates obtained by capacity spectrum method, time history analysis of the structure is performed subjecting it to pulse ground motions. The coherent part of velocity pulse of the ground motion can be represented (Papageorgiou and Mavroeidis 2003) by equation (2.2).Acceleration pulse can be obtained by differentiating Equation (2.2)

$$v(t) = A\left[\frac{1}{2}\left(1+\cos\left(\frac{\bar{t}}{\gamma}\right)\right)\cos\left(\bar{t}+\nu\right)\right] \quad , \; -\pi\gamma \le \bar{t} \le \pi\gamma \;\; with \;\gamma > 1 \tag{2.2}$$

$$\bar{t} = 2\pi f_p\left(t - t_o\right)$$

$$f_p = \frac{1}{T_p} \text{ where } T_p = \text{Pulse Duration}$$

$$\omega_p = \frac{2\pi}{T_p}$$

From Equation (2.2) it can be seen that the peak of velocity time history is A, therefore we can write $PGV = A$. Once the velocity pulse is defined, the acceleration and displacement pulse can be obtained by differentiating and integrating the velocity pulse respectively .Thus we can write

$$PGD = \frac{A}{\omega_p} = \frac{PGV}{\omega_p}$$

$$PGA = A\omega_p = PGV \cdot \omega_p$$

These can be combined and written as

$$PGV = \omega_p \cdot PGD = \frac{PGA}{\omega_p} \tag{2.3}$$

Divide Equation (2.1) by Equation (2.3)

$$\frac{PSV_y}{PGV} = \frac{\omega_n SD_y}{\omega_p \cdot PGD} = \frac{\frac{PSA_y}{\omega_n}}{\frac{PGA}{\omega_p}}$$

$$\Rightarrow \frac{PSV_y}{PGV} = \left(\frac{\omega_n}{\omega_p}\right)\frac{SD_y}{PGD} = \left(\frac{\omega_p}{\omega_n}\right)\frac{PSA_y}{PGA} \tag{2.4}$$

Now

$$\left(\frac{\omega_p}{\omega_n}\right) = \frac{\frac{2\pi}{T_p}}{\frac{2\pi}{T_n}} = \frac{T_n}{T_p}$$

if

$$d_y = \frac{SD_y}{PGD}\ ,\ v_y = \frac{PSV_y}{PGV}\ , a_y = \frac{PSA_y}{PGA}\ and\ t = \frac{T_n}{T_p}$$

Then Equation (2.4) can be written as

$$v_y = \frac{d_y}{t} = a_y t \tag{2.5}$$

Thus Equation (2.5) can be used to construct the Idealized Velocity Spectra

2.2.2 Response spectrum Co-ordinates

Using Equation (2.5) **and Figure 2.2**

The segment ab' is characterized by $a_y = 1$

$$\left(v_y\right)_{ab'} = \left(a_y = 1\right)\cdot t$$

Thus

Point a $t_a = \left(\frac{T_n}{T_p}\right)_a$

$$\left(v_y\right)_a = t_a$$

Point b $t_b = \left(\frac{T_n}{T_p}\right)_b$

$$\left(v_y\right)_{b'} = t_b$$

$$\left(v_y\right)_b = \alpha_{V,b}\left(v_y\right)_{b'}$$

Segment c"d' is characterized by $v_y = 1$

Point c

$$\left(v_y\right)_c = \alpha_{V,cd}\left(v_y\right)_{c"} = \alpha_{V,cd}$$

Point d

$$\left(v_y\right)_d = \alpha_{V,cd}\left(v_y\right)_{d'} = \alpha_{V,cd}$$

The segment beyond f i.e for $\frac{T_n}{T_p} > \left(\frac{T_n}{T_p}\right)_f$ is characterized by $d_y = 1$

Point f $t_f = \left(\frac{T_n}{T_p}\right)_f$

$$\left(v_y\right)_f = \frac{\left(d_y\right)_f}{t_f} = \frac{1}{t_f}$$

Figure 2.3 shows the generated idealized, normalized pseudo velocity Vs Normalized Period spectra. The spectra are generated for three magnitude ranges, plotted on log-log chart

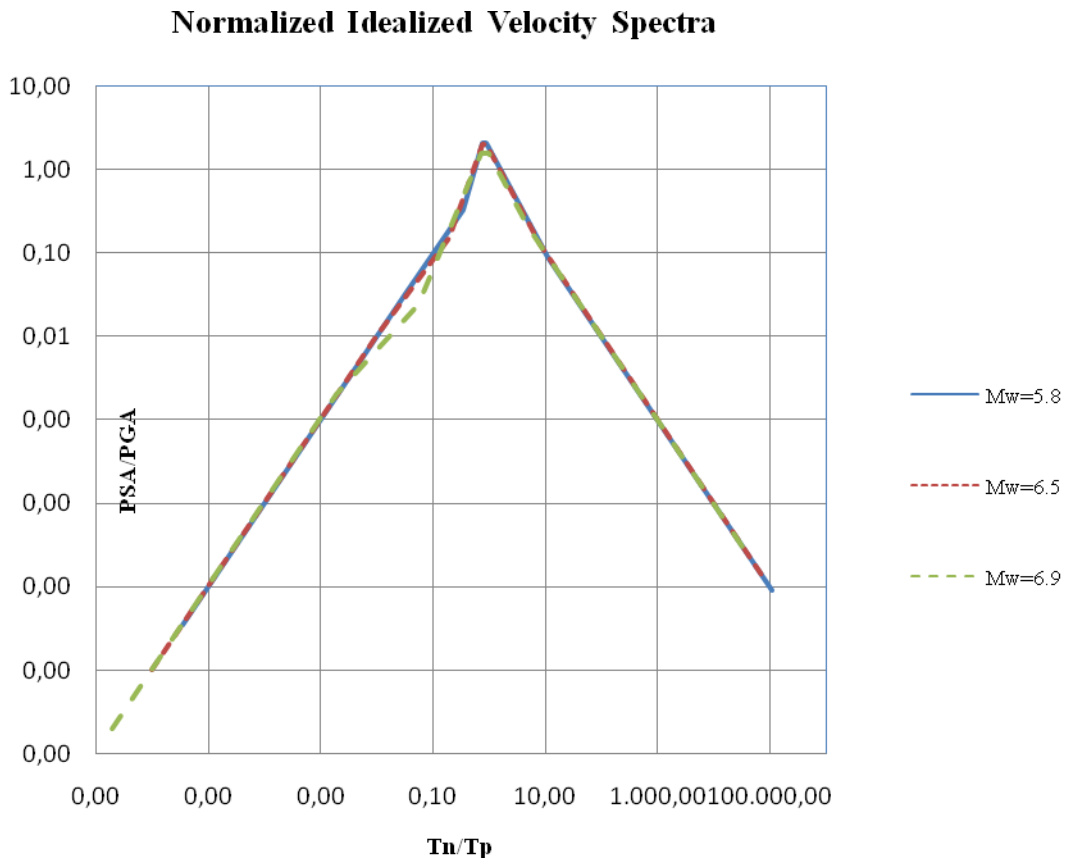

Figure 2-3 Generated Elastic Response Spectra

2.2.3 Generation of Equal ductility Response Spectrum

Ductility reduction factors are used to obtain constant ductility design spectrum. The reduction factors are as given by Papageorgiou et.al 2004

$$\left(\frac{T_n}{T_p}\right)_{c'} = \frac{\sqrt{2\mu-1}}{\mu}\left(\frac{T_n}{T_p}\right)_c$$

$$R_y = \begin{cases} 1, & \frac{T_n}{T_p} < \left(\frac{T_n}{T_p}\right)_a \\ \sqrt{2\mu-1}, & \left(\frac{T_n}{T_p}\right)_b < \frac{T_n}{T_p} < \left(\frac{T_n}{T_p}\right)_{c'} \\ \mu, & \frac{T_n}{T_p} > \left(\frac{T_n}{T_p}\right)_f \end{cases}$$

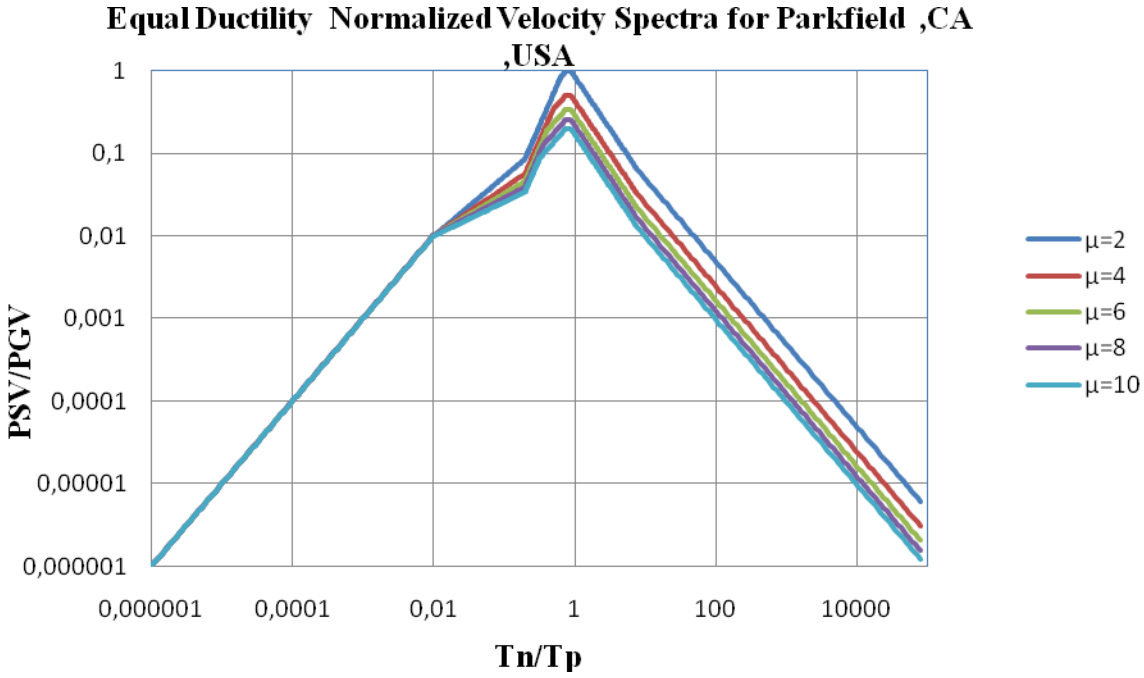

Figure 2-4 Generated constant Ductility Velocity Spectra

2.3 Generation of Demand Diagrams

A Demand diagram is a plot of Acceleration vs Ultimate Displacement, and is obtained as follows

$$SD_y = d_y\left(\frac{A}{\omega_p}\right)$$

Thus $SD_u = \mu \cdot SD_y$ (2.6)

$$PSA_y = a_y\left(A\omega_p\right)$$

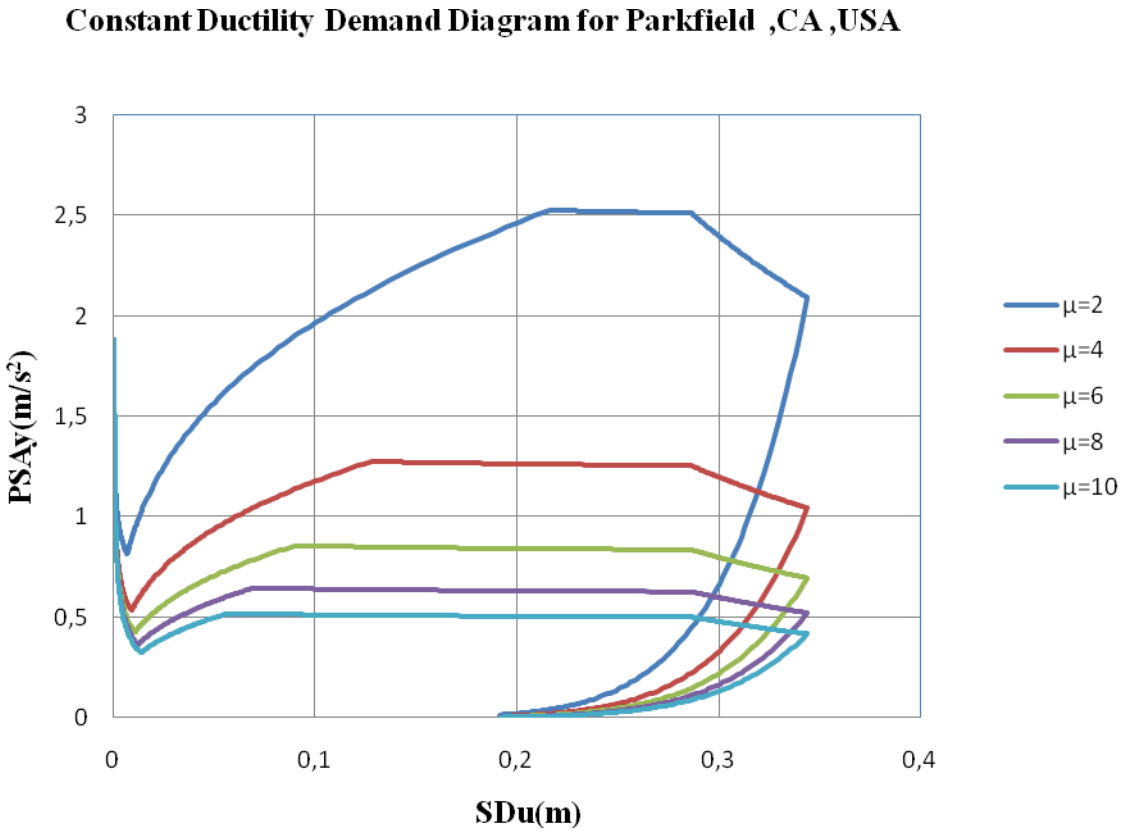

Figure 2-5 Generated Equal Ductility Demand Diagram

2.4 Summary:

In this chapter, a procedure for generating Constant ductility demand diagram has been outlined. At first the co-ordinates of the idealized normalized elastic velocity spectra were determined. Then the Idealized velocity spectra curve was reduced using ductility reduction factors to obtain constant ductility normalized velocity spectra. Then using these spectral ordinates, constant

ductility demand diagrams were generated. These demand diagrams will be used to determine structural capacity using capacity spectrum method.

3 Near Fault Ground Motion Pulse

3.1 Introduction

It has been observed that near-fault ground motions are frequently characterized by intense velocity and displacement pulses. These pulses impose severe demands on the structures constructed in near fault regions. These pulses are of relatively longer period which makes near-fault ground motion different from far-field ground motion. Since the time these observations were made, attempts to represent these pulses using mathematical models were being made by the research community. A mathematical model proposed by Papageorgiou et.al. 2004 is used in this work to generate a set of near-fault ground motion pulses. These pulse excitations will be used in time history analysis.

3.2 Mathematical model for near-fault ground motion

The mathematical model for the velocity pulse is

$$v(t)=\begin{cases} A\frac{1}{2}\left(1+\cos\left(\frac{2\pi f_p}{\gamma}(t-t_o)\right)\right)\cos\left[2\pi f_p(t-t_o)+\nu\right], \\ t_o-\frac{\gamma}{2f_p}\le t\le t_o+\frac{\gamma}{2f_p} \quad \text{With } \gamma>1 \\ 0, \qquad\qquad\qquad\qquad \text{Otherwise} \end{cases} \tag{3.1}$$

Where

A=Amplitude or PGV

f_p = Prevailing frequency

ν = Phase angle

γ = Oscillatory Character

The acceleration pulse can be represented as

$$a(t)=\begin{cases} -\dfrac{A\pi f_p}{\gamma}\left[\begin{array}{l}\sin\left(\dfrac{2\pi f_p}{\gamma}(t-t_o)\right)\cos\left[2\pi f_p(t-t_o)+\nu\right] \\ +\gamma\sin\left[2\pi f_p(t-t_o)+\nu\right]\left[1+\cos\left(\dfrac{2\pi f_p}{\gamma}(t-t_o)\right)\right]\end{array}\right] \\ t_o-\dfrac{\gamma}{2f_p}\le t\le t_o+\dfrac{\gamma}{2f_p} \\ \text{With } \gamma>1 \\ 0, \qquad \text{Otherwise}\end{cases} \tag{3.2}$$

Values of the input parameters have been determined by fitting the analytical model to near-fault ground motion records by Papageorgiou et.al. 2004, for a set of ground motion records. Some of the ground motion records are reproduced using these parameters for use in time history analysis.

Table 3.1 Parameters used for reproducing Near fault Ground motion records

No	Location	Station	Component	A	γ	$\nu(^o)$	$f_p\,(Hz)$	t_o (s)
1	Parkfield,CA,USA	C02	SN	60	1.7	100	0.5	4.1
2	San Fernado,CA,USA	PCD	SN	115	1.6	180	0.68	3
3	Gazli,USSR	KAR	Rad	45	2.9	70	0.238	8.4
4	Bucharest,Romania	BRI	SN	62	2.4	200	0.47	3.83
5	Tabas,Iran	TAB	SP	104	2.2	180	0.19	12.4
6	Coyote Lake,CA,USA	GA6	SN	48	1.55	315	1	2.6
7	Imperial Valley, CA,USA	E04	SN	71	1.9	305	0.225	6.1
8		E05	SN	84	1.9	300	0.255	6.6
9		E06	SN	96	2.1	265	0.26	6.35
10		E07	SN	79	2.1	25	0.275	6.1
11		EMO	SN	78	2.3	0	0.34	4.95

Acceleration and velocity pulses representing Parkfield earthquake ground motion pulse are presented below.

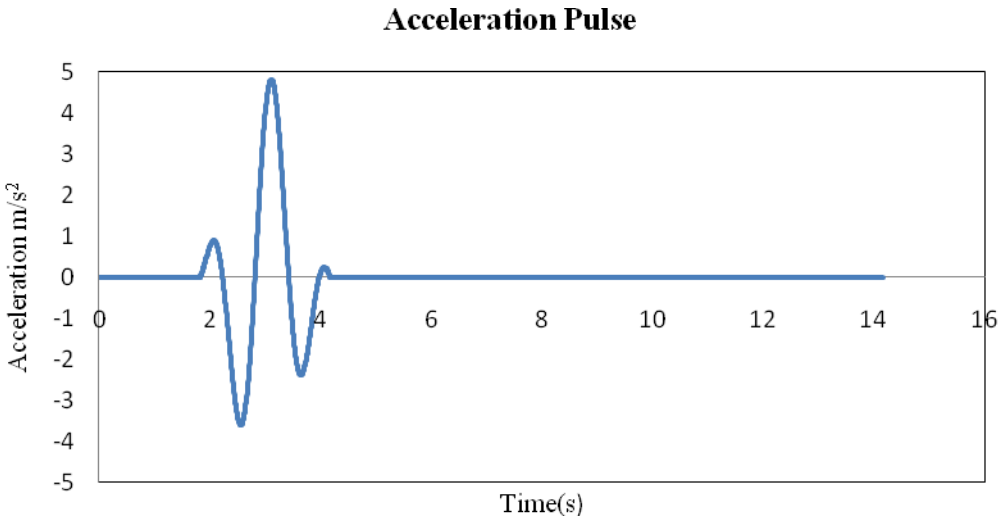

Figure 3-1 Acceleration Pulse , Parkfield , CA,USA

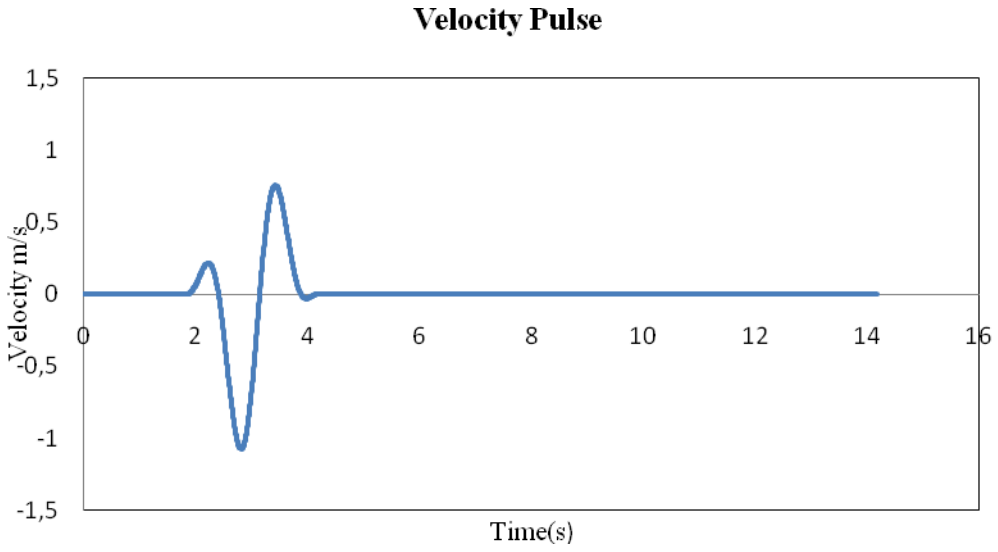

Figure 3-2 Velocity Pulse, Parkfield, CA, USA

4 Capacity Curve

4.1 Introduction

A pushover curve is generated by subjecting a detailed or a carefully simplified structural model to one or more lateral load patterns and then increasing the magnitude of the total load to generate a nonlinear inelastic force-deformation relationship. The load vector is usually a representation of the load acting on the structure vibrating in its first mode .In ATC-40 Procedure A , the global parameters used are spectral acceleration and spectral displacement. Therefore a Capacity curve used in this procedure is a curve obtained by transforming the structure base shear vs. roof displacement curve into an Equivalent Single Degree of Freedom structure, acceleration vs. displacement curve .The equivalent SDOF properties correspond to the first mode properties of the detailed structure .In this chapter equations needed to convert the pushover curve into a capacity curve will be developed.

4.2 Equivalent SDOF

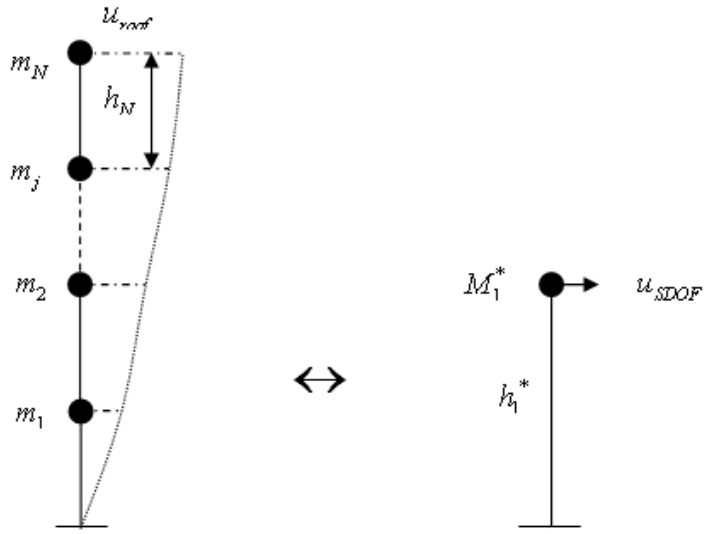

Figure 4-1 MDOF system to an equivalent SDOF system

4.2.1 Equivalent Displacement

Equations of motion for Equivalent SDOF

$$M_1^* \ddot{u}_{SDOF} + C\dot{u}_{SDOF} + Ku_{SDOF} = -M_1^* \ddot{u}_g$$

Divide by M_1^*

$$\ddot{u}_{SDOF} + 2\zeta\omega_1\dot{u}_{SDOF} + \omega_1^2 u_{SDOF} = -\ddot{u}_g \tag{4.1}$$

Equation of motion for MDOF

$$\mathbf{M}\ddot{\mathbf{u}} + \mathbf{C}\dot{\mathbf{u}} + \mathbf{K}\mathbf{u} = -\mathbf{M}\mathbf{i}\ddot{u}_g$$

$$\mathbf{u} = \boldsymbol{\phi}\mathbf{q}$$

$$\mathbf{M}\boldsymbol{\phi}\ddot{\mathbf{q}} + \mathbf{C}\boldsymbol{\phi}\dot{\mathbf{q}} + \mathbf{K}\boldsymbol{\phi}\mathbf{q} = -\mathbf{M}\mathbf{i}\ddot{u}_g$$

Multiplying both sides with $\boldsymbol{\phi}_n^T$

$$\boldsymbol{\phi}_n^T\mathbf{M}\boldsymbol{\phi}\ddot{\mathbf{q}} + \boldsymbol{\phi}_n^T\mathbf{C}\boldsymbol{\phi}\dot{\mathbf{q}} + \boldsymbol{\phi}_n^T\mathbf{K}\boldsymbol{\phi}\mathbf{q} = -\boldsymbol{\phi}_n^T\mathbf{M}\mathbf{i}\ddot{u}_g$$

Due to orthogonality

$$\boldsymbol{\phi}_n^T\mathbf{M}\boldsymbol{\phi} = \boldsymbol{\phi}_n^T\mathbf{M}\boldsymbol{\phi}_n \quad , \boldsymbol{\phi}_n^T\mathbf{C}\boldsymbol{\phi} = \boldsymbol{\phi}_n^T\mathbf{C}\boldsymbol{\phi}_n \quad , \boldsymbol{\phi}_n^T\mathbf{K}\boldsymbol{\phi} = \boldsymbol{\phi}_n^T\mathbf{K}\boldsymbol{\phi}_n$$

$$\therefore \boldsymbol{\phi}_n^T\mathbf{M}\boldsymbol{\phi}_n\ddot{q}_n + \boldsymbol{\phi}_n^T\mathbf{C}\boldsymbol{\phi}_n\dot{q}_n + \boldsymbol{\phi}_n^T\mathbf{K}\boldsymbol{\phi}_n q_n = -\boldsymbol{\phi}_n^T\mathbf{M}\mathbf{i}\ddot{u}_g$$

Now if $M_n = \boldsymbol{\phi}_n^T\mathbf{M}\boldsymbol{\phi}_n$, $\boldsymbol{\phi}_n^T\mathbf{C}\boldsymbol{\phi}_n = C_n = 2\zeta_n M_n\omega_n$, $\boldsymbol{\phi}_n^T\mathbf{K}\boldsymbol{\phi}_n = K_n = \omega_n^2 M_n$

$$\Gamma_n = \frac{-\boldsymbol{\phi}_n^T\mathbf{M}\mathbf{i}}{\boldsymbol{\phi}_n^T\mathbf{M}\boldsymbol{\phi}_n}$$

Then we can write the equation of motion as

$$\ddot{q}_n + 2\zeta_n\omega_n\dot{q}_n + \omega_n^2 q_n = -\Gamma_n\ddot{u}_g$$

For a system oscillating in the n-th mode

$$u_{roof} = \phi_{roof} q_n$$

$$\therefore \phi_{roof}\ddot{q}_n + 2\zeta_n\omega_n\phi_{roof}\dot{q}_n + \omega_n^2\phi_{roof} q_n = -\Gamma_n\phi_{roof}\ddot{u}_g$$

$$\Rightarrow \ddot{u}_{roof} + 2\zeta_n\omega_n\dot{u}_{roof} + \omega_n^2 u_{roof} = -\Gamma_n\phi_{roof}\ddot{u}_g$$

$$\Rightarrow \frac{\ddot{u}_{roof}}{\Gamma_n\phi_{roof}} + 2\zeta_n\omega_n\frac{\dot{u}_{roof}}{\Gamma_n\phi_{roof}} + \omega_n^2\frac{u_{roof}}{\Gamma_n\phi_{roof}} = -\ddot{u}_g$$

Comparing with equation (4.1) we can write

$$u_{SDOF} = \frac{u_{roof}}{\Gamma_n\phi_{roof}} = D_n(t)$$

Therefore for a SDOF vibrating with fundamental frequency

$$u_{SDOF} = D_1(t) = \frac{u_{roof}}{\Gamma_1 \phi_{roof}} \quad \text{and} \quad \ddot{D}_1(t) + 2\zeta_n \omega_n \dot{D}_1(t) + \omega_n^2 D_1(t) = -\ddot{u}_g \tag{4.2}$$

4.2.2 Equivalent Lateral force

From equation (4.2) we can write

$$\mathbf{u_1} = \Gamma_1 \begin{Bmatrix} \phi_{1N} \\ . \\ . \\ \phi_{12} \\ \phi_{11} \end{Bmatrix} D_1(t)$$

Also Pseudo acceleration at each floor

$$\mathbf{A_1} = \omega_1^2 \mathbf{u_1} = \Gamma_1 \begin{Bmatrix} \phi_{1N} \\ . \\ . \\ \phi_{12} \\ \phi_{11} \end{Bmatrix} \omega_1^2 D_1(t) = \Gamma_1 \begin{Bmatrix} \phi_{1N} \\ . \\ . \\ \phi_{12} \\ \phi_{11} \end{Bmatrix} A_{SDOF}(t)$$

Force at each floor

$$\mathbf{f_1} = \mathbf{M A_1} = \Gamma_1 \begin{Bmatrix} m_N \phi_{1N} \\ . \\ . \\ m_2 \phi_{12} \\ m_1 \phi_{11} \end{Bmatrix} A_{SDOF}(t)$$

Hence the total force acting on the MDOF structure vibrating in the first mode is

$$\mathrm{F}_1 = \Gamma_1 A_{SDOF}(t) \sum_{n=1}^{N} m_n \phi_{1n}$$

Where

$$\Gamma_1 = \frac{\sum_{n=1}^{N} m_n \phi_{1n}}{\sum_{n=1}^{N} m_n \phi_{1n}^{\ 2}}$$

$$\therefore \mathrm{F}_1 = A_{SDOF}(t)\cdot\Gamma_1\sum_{n=1}^{N} m_n\phi_{1n} = A_{SDOF}(t)\cdot\frac{\sum_{n=1}^{N} m_n\phi_{1n}}{\sum_{n=1}^{N} m_n{\phi_{1n}}^2}\cdot\sum_{n=1}^{N} m_n\phi_{1n} = A_{SDOF}(t)\frac{\left(\sum_{n=1}^{N} m_n\phi_{1n}\right)^2}{\sum_{n=1}^{N} m_n{\phi_{1n}}^2}$$

Referring to figure 4.1

$$\mathrm{F}_1 = A_{SDOF}(t)\frac{\left(\sum_{n=1}^{N} m_n\phi_{1n}\right)^2}{\sum_{n=1}^{N} m_n{\phi_{1n}}^2} = A_{SDOF}(t)M_1^*$$

This gives us

$$M_1^* = \frac{\left(\sum_{n=1}^{N} m_n\phi_{1n}\right)^2}{\sum_{n=1}^{N} m_n{\phi_{1n}}^2} \tag{4.3}$$

4.3 Conversion of Pushover curve to Capacity curve

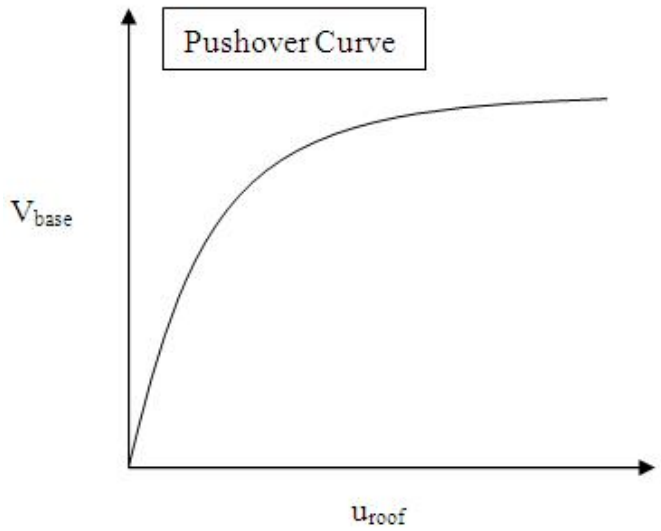

Figure 4-2 Pushover Curve

Using equations (4.2) and (4.3)

$$A_{SDOF} = \frac{V_{base}}{M_1^*} = \frac{V_{base}}{\frac{\left(\sum_{n=1}^{N} m_n \phi_{1n}\right)^2}{\sum_{n=1}^{N} m_n \phi_{1n}^2}} \qquad u_{SDOF} = \frac{u_{roof}}{\Gamma_1 \phi_{roof}}$$

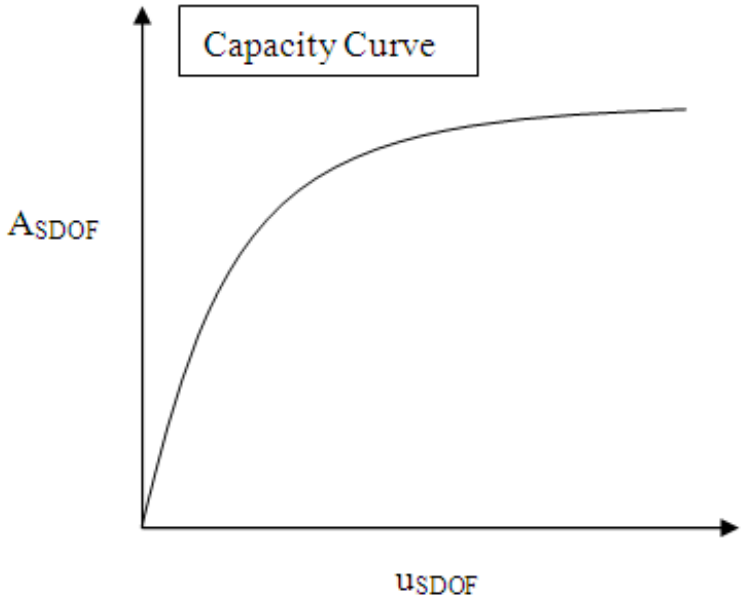

Figure 4-3 Capacity Curve

It should be noted that though modal analysis is valid only till the structure is elastic, dynamic properties can effectively be represented by modes of vibration and structural period of the corresponding system. (Chopra2007)

Sample pushover curve and capacity curve are presented below for three storey LA structure

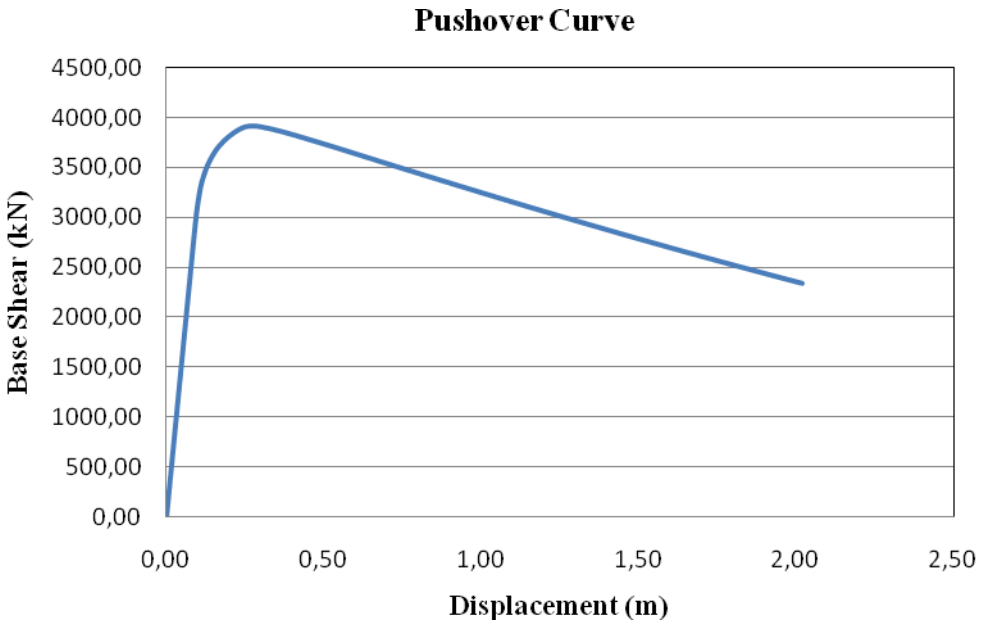

Figure 4-4 Pushover curve for 3 Storey LA Pre-Northridge SAC building

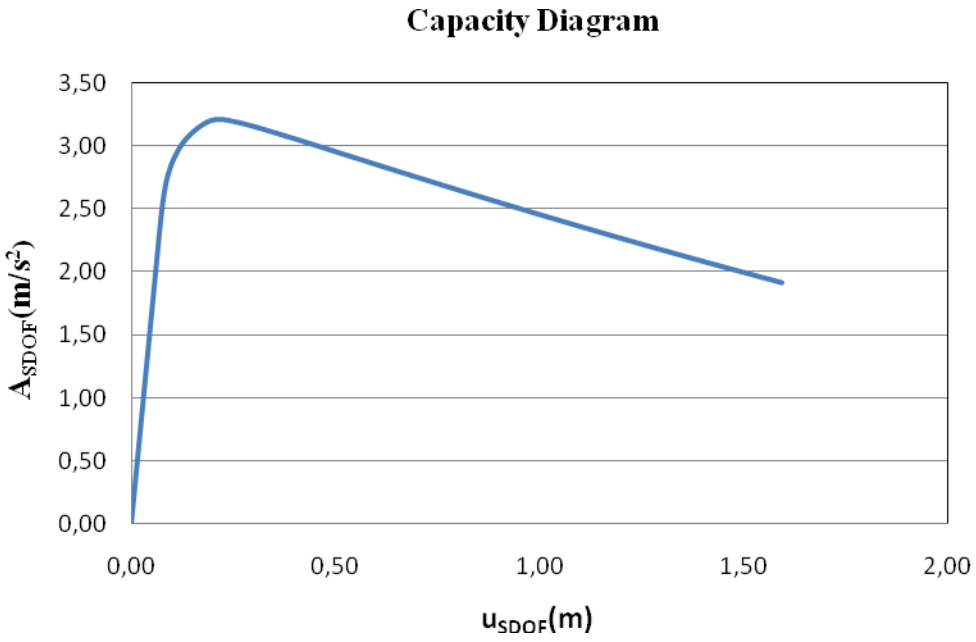

Figure 4-5 Capacity curve for 3 Storey LA Pre-Northridge SAC building

5 Models for Analysis

5.1 Introduction

The buildings considered in this study are three-story steel buildings designed for Los Angles, Seattle and Boston as a part of the SAC project. The structural designs considered are Pre-Northridge designs. Details of these buildings are available in Gupta and Krawinkler (1999). These low-rise buildings have a fairly uniform distribution of stiffness as well as strength throughout their height, without any obvious soft and/or weak story condition. The Los Angeles (LA) and Seattle (SE) structures have been designed following UBC 1994. Boston (BO) structure has been designed following BOCA1993.The buildings have been designed as standard office buildings situated on stiff soil (soil type S2 as per UBC '94 and BOCA '93 definitions).The capacity of these structures is evaluated using the capacity spectrum method with a only modification that the Demand diagrams are generated using constant ductility response spectra. These results are checked against Dynamic pushover analysis results.

5.2 Types of analysis used

5.2.1 Pushover analysis

Conventional (non-adaptive) pushover analysis is utilised in this study to estimate the horizontal capacity of structures featuring a dynamic response that is not significantly affected by the levels of deformation incurred (i.e. the horizontal load pattern, which aims at simulating dynamic response, can be assumed as constant).

The applied incremental load P is kept proportional to the pattern of nominal loads (P^o) initially defined by the user: $P = \lambda P^o$. The load factor λ is automatically increased by the program until a user-defined limit, or numerical failure, is reached. For the incrementation of the loading factor, different strategies may be employed using seismostruct,

- *Load control* refers to the case where the load factor is directly incremented and the global structural displacements are determined at each load factor level.
- *Response control* refers to direct incrementation of the global displacement of one node and the calculation of the loading factor that corresponds to this displacement.

- *Automatic response control* refers to a procedure in which the loading increment is automatically adjusted by SeismoStruct, depending on the convergence conditions at the previous step.

In this study a response control incrementation of loading factor has been adopted

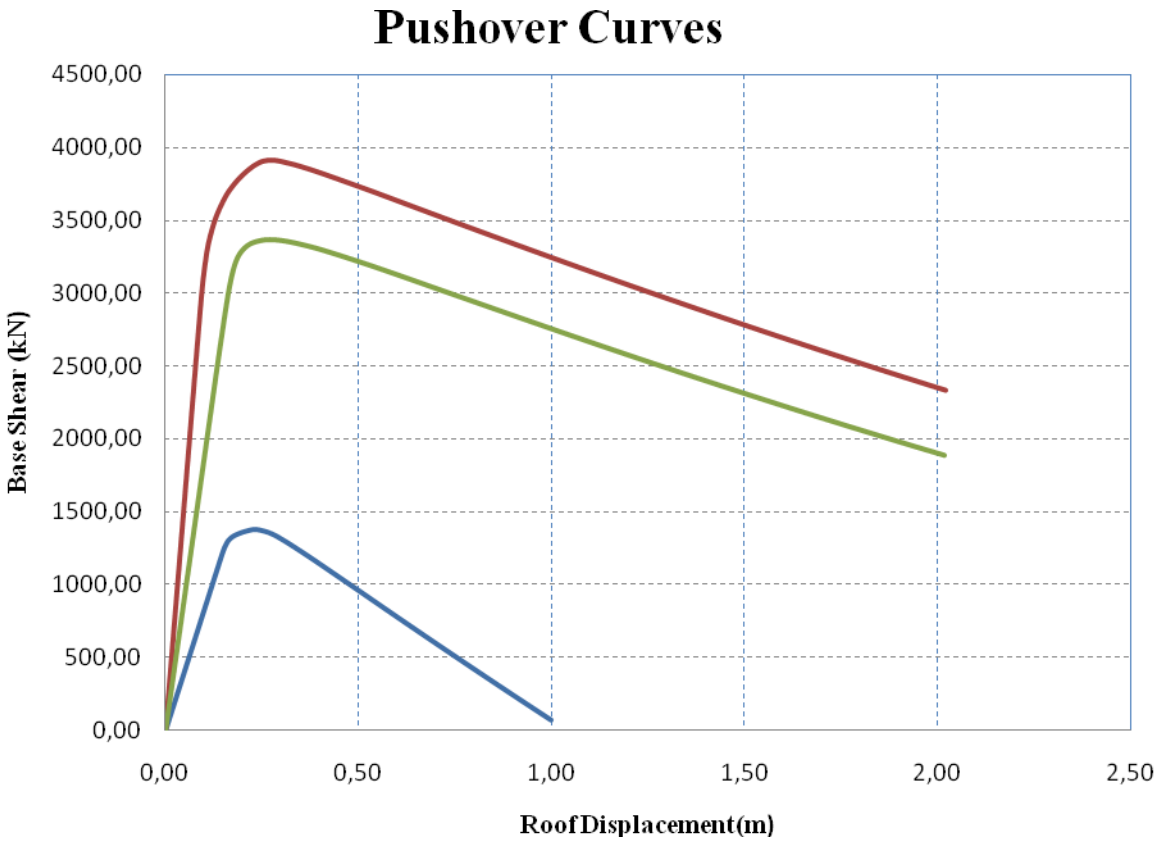

Figure 5-1 Pushover curves ,considering P-Delta effects for a bilinear model with 3% strain hardening

5.2.2 Dynamic time history analysis

Dynamic analysis is commonly used to predict the nonlinear inelastic response of a structure subjected to earthquake loading. In this study the structure is subjected to near-fault ground motion pulses discussed in chapter 3

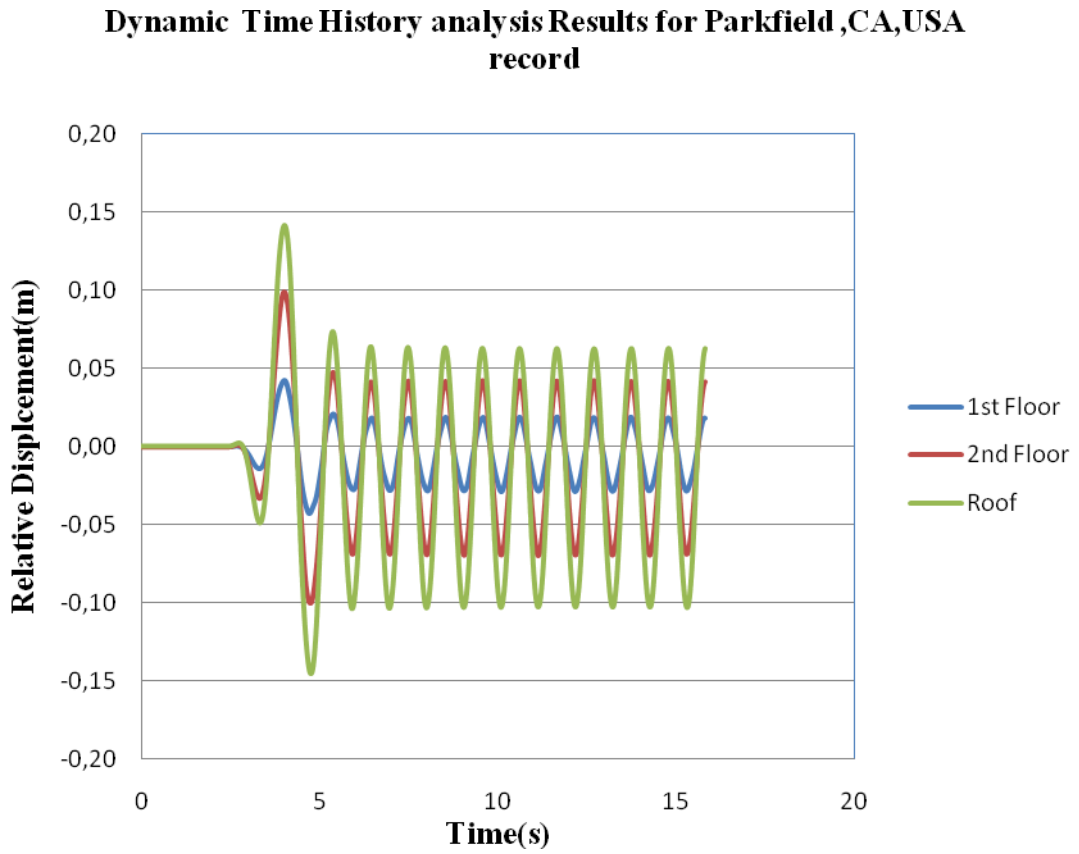

Figure 5-2 Time history results, considering P-Delta effect for a elastoplastic Stress Strain model

5.3 Loads applied

Seismic weights as in Gupta and Krawlinkler (1999) have been applied. The seismic weights Per frame are as follows

Roof : 517 tonnes
Floor 3 and Floor 2: 478 tonnes

For 3 Storey Pre-Northridge LA structure seismic weights distributed equally between three bays, where as for Seattle and Boston structures it is distributed equally for four bays .This gives Seismic weights for each bay as

For Los-Angeles structure for each bay
Roof : 172 tonnes
Floor 3 and Floor 2 : 159 tonnes

For Seattle and Boston structures for each bay

Roof : 129 tonnes
Floor 3 and Floor 2 : 119 tonnes

Floor dead load for weight calculations: 4596.48 N/mm^2
Roof dead load excluding penthouse: 3974.04 N/mm^2
Penthouse dead load: 5554.08 N/mm^2
Reduced live load per floor and for roof: 957.6 N/mm^2

This gives the following total P-Delta load

Roof level 5413 kN
Floor 3 and Floor 2 5573 kN

5.4 P-Delta effect

Since the moment resisting frame carries negligible gravity load, no gravity load is applied to the Moment resisting frames (MRF) .The effect of gravity loads is considered in evaluating P-Delta effect. A dummy column with very high axial stiffness and negligible bending stiffness is attached to the frame using links so that the link doesn't transfer moment and shear of the external column to the structure, but only the displacements .A simple illustration of this mechanism and related equations are presented below.

From figure (5.3 a) which is a vertical cantilever we can write the following equation

$$M = hH + P\Delta \tag{5.1}$$

From figure (5.3 b) in which a dummy column is attached to the vertical cantilever with a truss element, the equilibrium equations for the dummy column can be written as

$$P\Delta = Rh$$

$$R = \frac{P\Delta}{h}$$

Thus the above force is transferred to the vertical cantilever by the rigid link .Therefore the total moment at the base of the vertical cantilever is

$$M = Hh + \frac{P\Delta}{h}h = Hh + P\Delta$$

Which is same as equation (5.1)
Therefore introduction of a dummy column with a high axial stiffness and negligible bending stiffness can be used to take care of P-Delta effects.

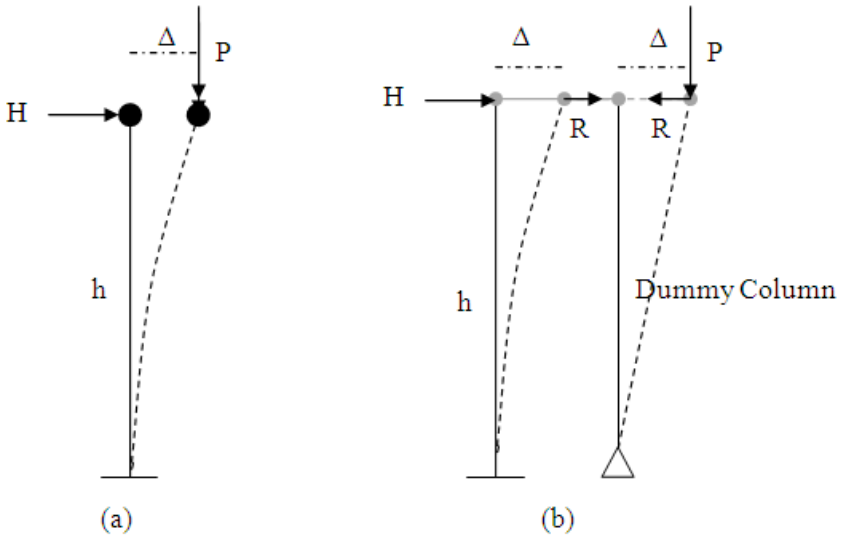

Figure 5-3 Use of a dummy column to incorporate P-Delta effects

5.5 Pushover load distribution

A lateral load pattern as in NEHRP 1994 has been applied .The load pattern is given by the following equation.

$$C_x = \frac{w_x h_x^{\,k}}{\sum_{n=1}^{n} w_i h_i^k}$$

where C_x is the normalized load at floor level x, w_i and w_x are the seismic weights at floor i and x respectively, h_i and h_x are the heights from the ground level to floor i and x, and k is a period-dependent factor. In this study a k value of 2 has been used for all pushover analysis.

5.6 Stress Strain Curve

A Elastic-perfectly plastic stress strain model has been adopted .The model is defined by the following parameters

- Modulus of elasticity - Es: This is the initial elastic stiffness of the material. Its value has been taken as 200Mpa
- Yield strength - fy: This is the stress at yield. Its value has been taken as 344737.9kpa for A572Gr50 , 248211.3kpa for A36 and 344737.9 kpa for A36GR50 Steel
- Strain hardening parameter-:This is the ratio between the post-yield stiffness (*Esp*) and the initial elastic stiffness (*Es*) of the material. The former is defined as $Esp=(f_{ult}-fy)/(\varepsilon_{ult}-fy/Es)$, where *fult* and ε_{ult} represent the ultimate or maximum stress and strain capacity

of the material, respectively. Its value is zero as the model adopted is elastic-perfectly plastic

- Specific weight-:This is the specific weight of the material. The default value is 78 kN/m^3.

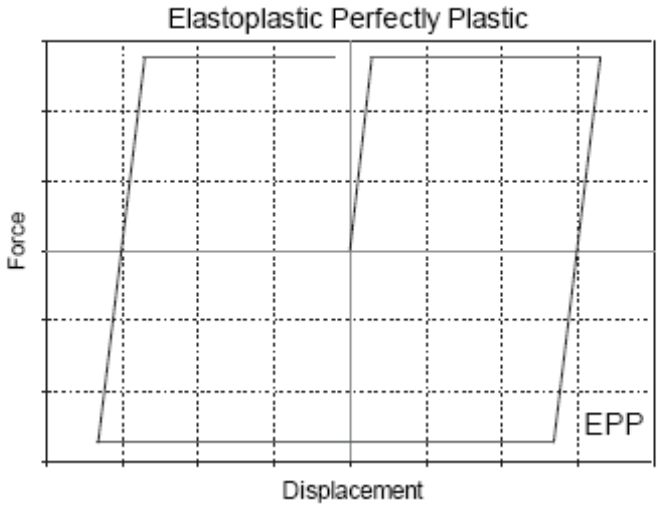

Figure 5-4 Elastic perfectly plastic model

5.7 Layout of SAC buildings

3 Storey LA Structures

Elevation

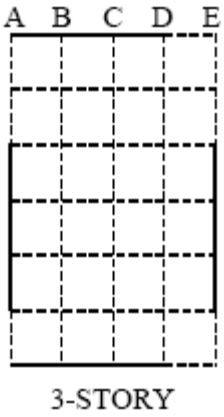

Plan

Moment resisting frames are represented in the plan with a thick line

3 Storey SE and BO Structures

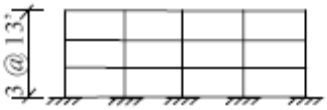

Elevation

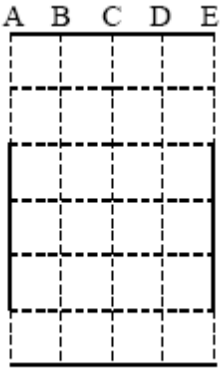

PLAN

Moment resisting frames are represented in the plan with a thick line

3 Storey LA Seismostruct model

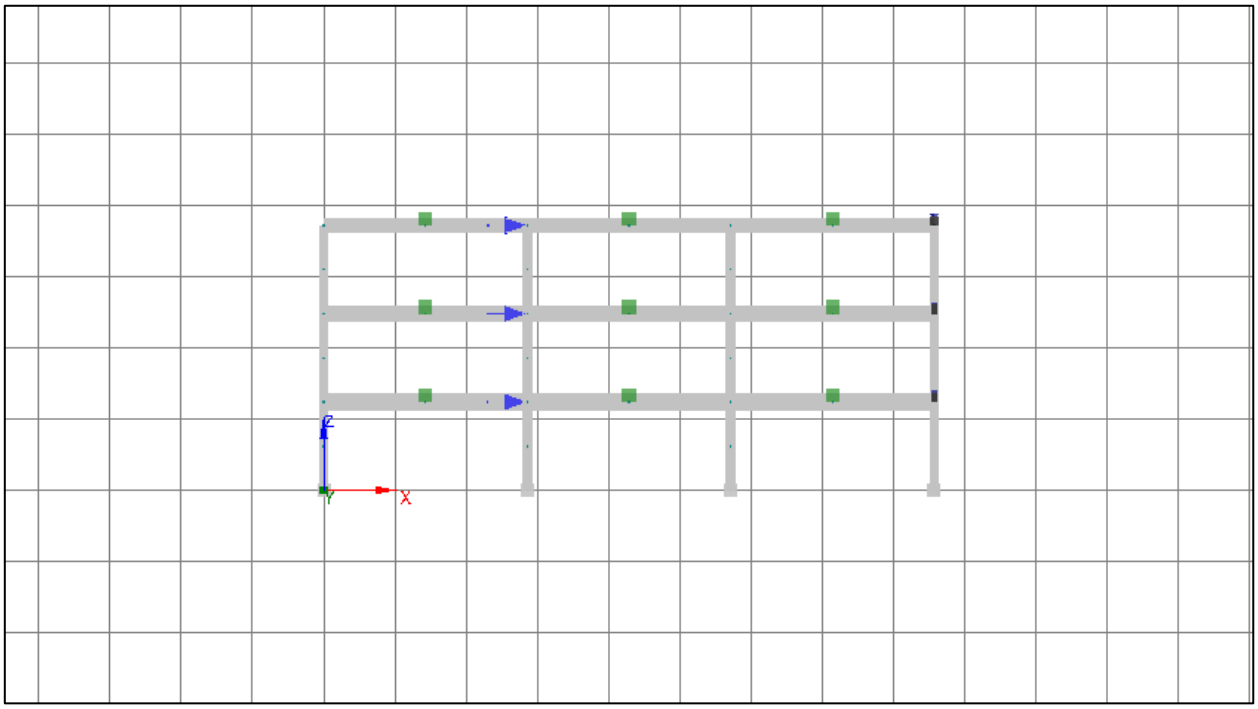

Figure 5-5 Storey LA MRF Seismostruct model

3 Storey SE and BO Seismostruct models

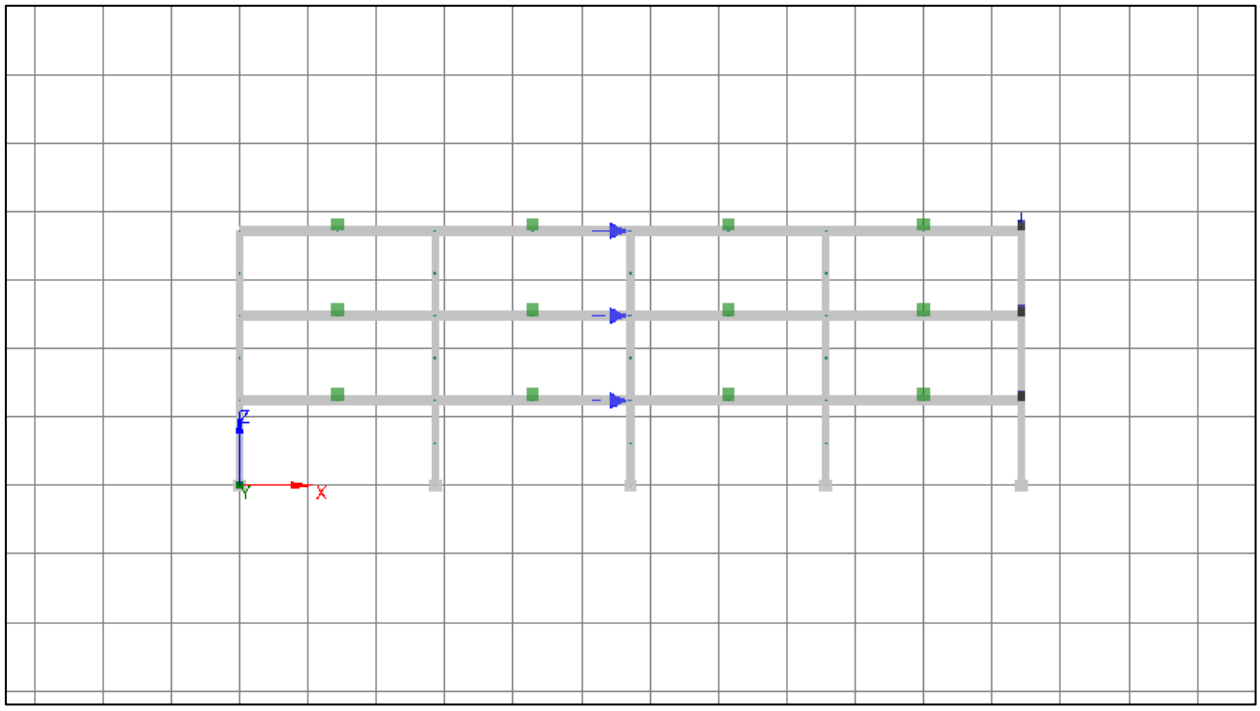

Figure 5-6 Storey SE and BO MRF Seismostruct model

6 Results and Conclusion

The primary objective of this study is to apply the capacity spectrum method to buildings subjected to near-fault ground motion .To implement the capacity spectrum method, constant ductility inelastic design spectra proposed by Papageorgiou and Mavroeidis 2004. have been used .The structural models used in this study are SAC 3 storey Pre-Northridge buildings designed for three different regions, Los-Angeles , Seattle and Boston. The results obtained by capacity spectrum method are compared with dynamic time history analysis results. The buildings were subjected to near fault ground motion pulse which can be reproduced using the mathematical model suggested by Papageorgiou and Mavroeidis 2003. In this chapter, analysis results have been presented and conclusions have been made.

6.1 Demand Diagram

Demand diagram as discussed in Chapter 2 is a plot of spectral acceleration vs. maximum deformation .Constant ductility normalized demand diagrams have been generated for three ranges of magnitude Mw 5.6-6.3, 6.4-6.7, 6. 8-7.6. The constant ductility normalized demand diagrams can be used to generate diagrams for specified Peak Ground Velocity (PGV) values.

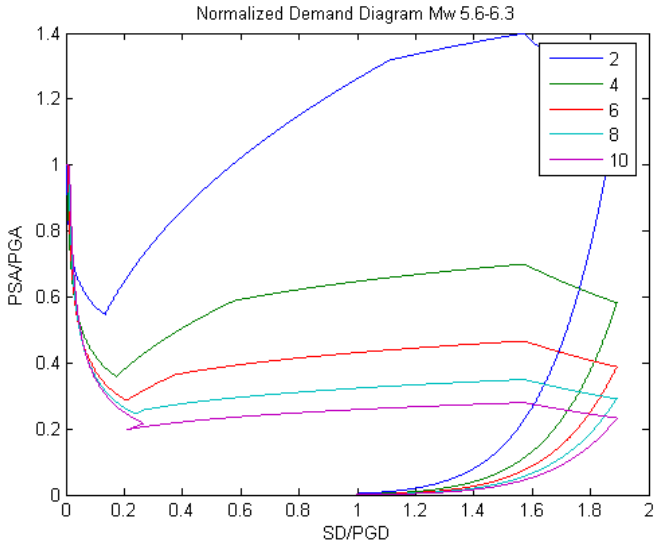

Figure 6-1 Normalized Demand Diagram for Earthquake moment magnitude 5.6-6.3

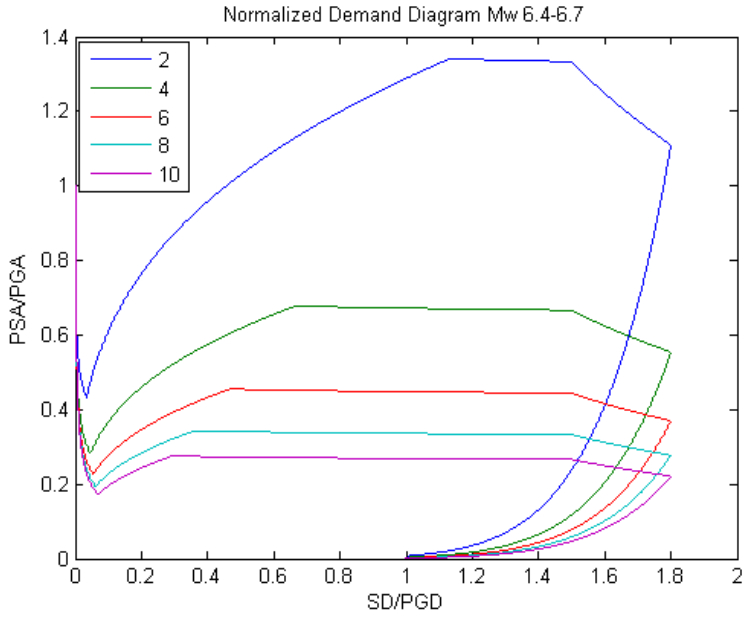

Figure 6-2 Normalized Demand Diagram for Earthquake moment magnitude 6.4-6.7

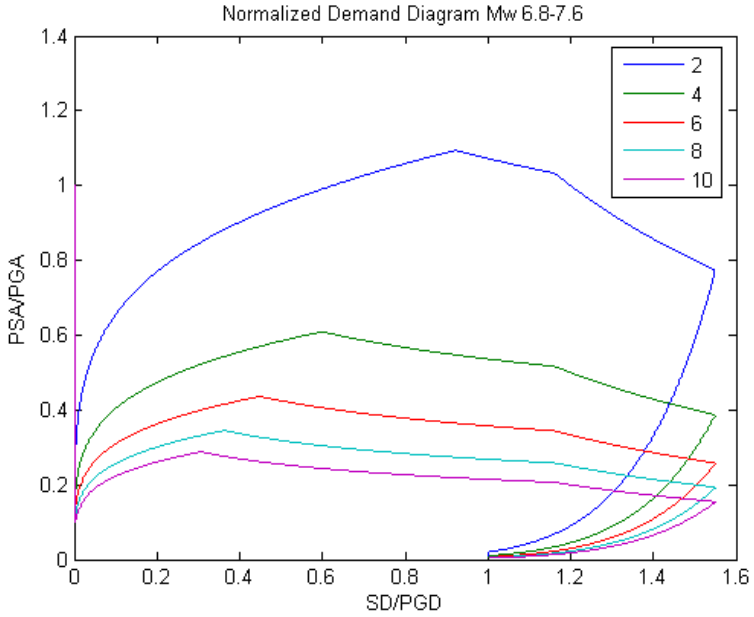

Figure 6-3Normalized Demand Diagram for Earthquake moment magnitude 6.8-7.6

The numbers in the legend indicate the ductility value for which the corresponding curve has been developed .Various segments of the constant ductility demand diagram are shown comparing it with the normalized velocity spectra .

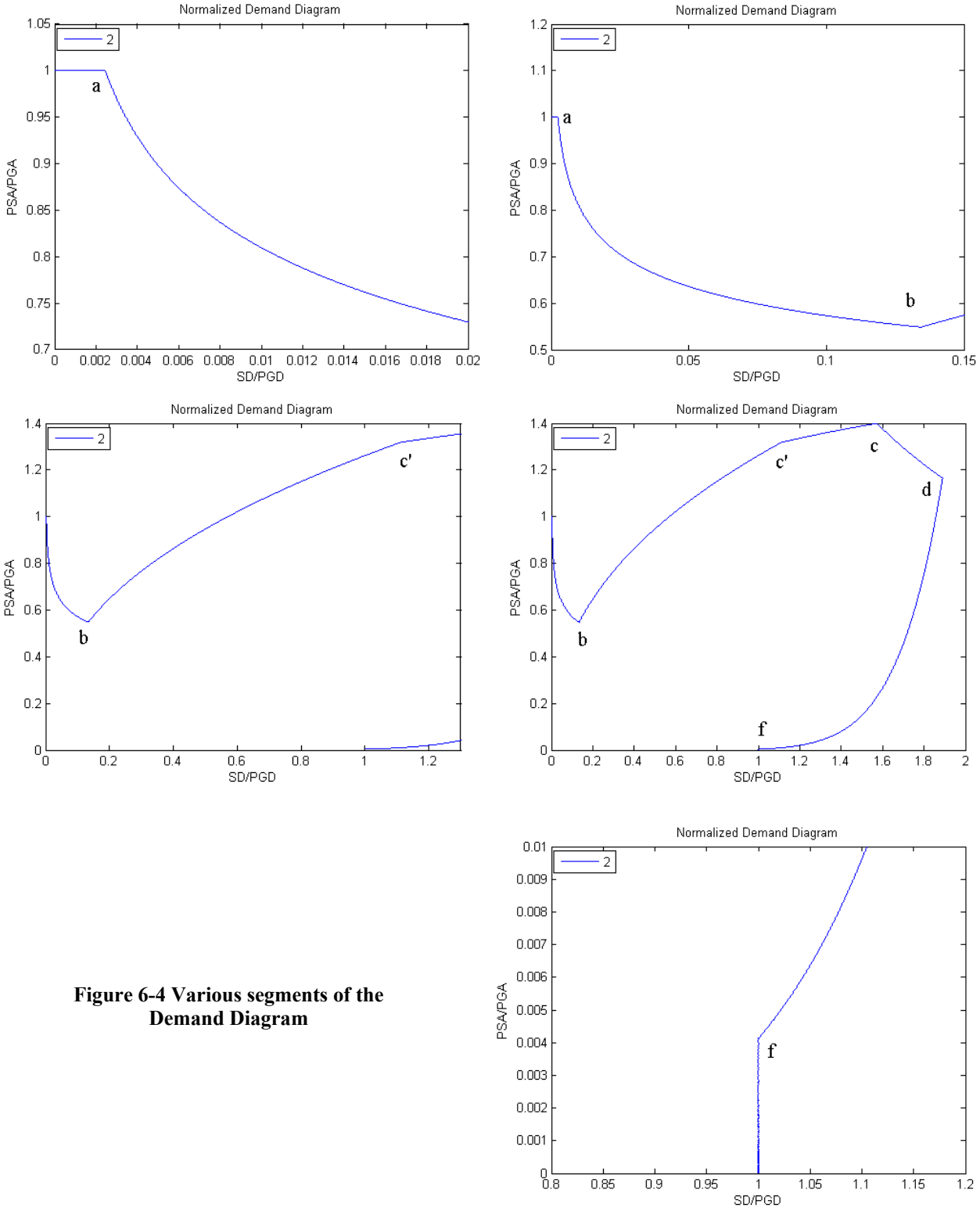

Figure 6-4 Various segments of the Demand Diagram

The segment before 'a' normal to acceleration axis is characterized by constant acceleration. The segment after 'f' is characterized by constant displacement. Segment cd is characterized by constant velocity. Observing figures 3.1 through 3.3 it can be said that segments c'c and cd are very sensitive to ductility.

6.2 Capacity curves

The capacity curves for the three structures used in analysis are shown below. The negative post yield stiffness is because of P-Delta effects.

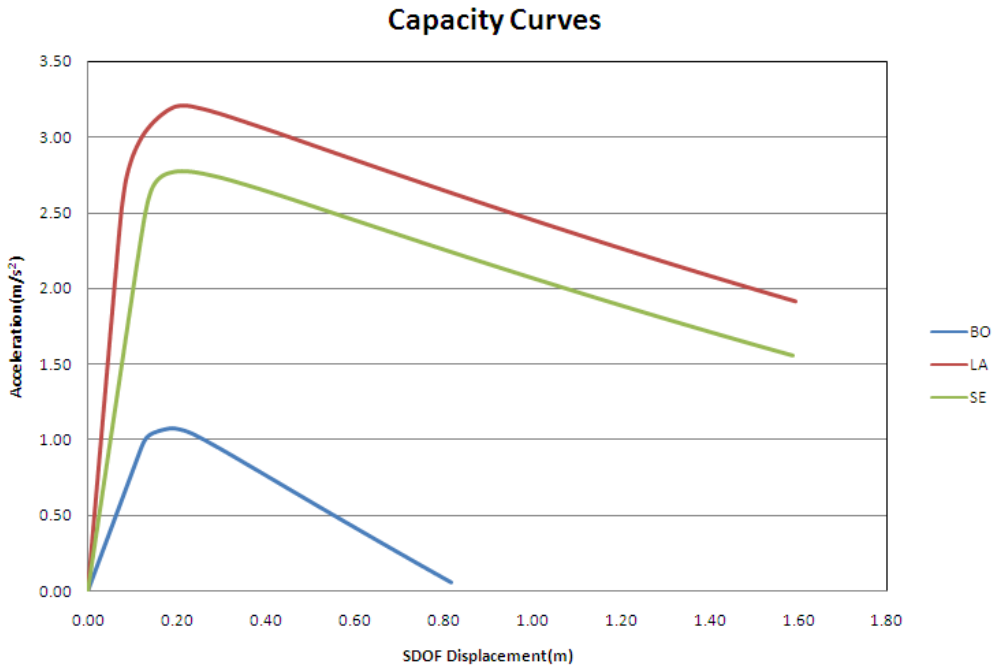

Figure 6-5 Capacity Curve of all the three structural models

These curves were generated from the pushover curves using two factors α_1 and α_2 which are defined as.

$$\alpha_1 = M_1^* = \frac{\left(\sum_{i=1}^{N} m_i \phi_{ip}\right)^2}{\sum_{i=1}^{N} m_i \phi_{ip}^{\ 2}}$$

$$\text{Acceleration} = \frac{V_{base}}{\alpha_1}$$

$$\alpha_2 = \frac{1}{\Gamma_1 \phi_{roof}}$$

$$\text{SDOF displacement} = \alpha_2 u_{roof}$$

Table 6-1 Conversion factors α_1 and α_2

Structure	α_1	α_2
LA	1220	0.789
SE	1210	0.788
BO	1280	0.817

The time history analysis displacement values are also converted to equivalent SDOF displacement for comparison with capacity spectrum analysis results

6.3 Comparison of capacity spectrum method and time history analysis results

In this section results of capacity spectrum method and time history analysis have been presented (Table 6.3 and Table 6.4 respectively). The percentage error is calculated with respect to time history analysis results. Therefore a negative percentage error indicates that the displacement values obtained by capacity spectrum method are larger than those obtained from time history analysis. A positive percentage indicates just the opposite. The case for which the system becomes unstable is marked as US. The capacity spectrum method does not indicate instability. It always gives a finite value for displacement.

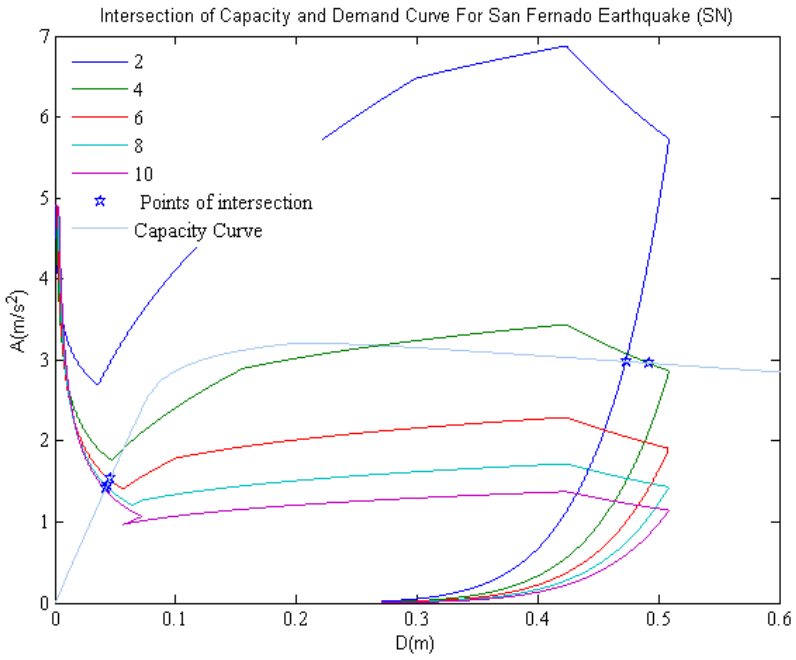

Figure 6-6 Intersection of capacity curve and demand diagram

Table 6-2 fundamental periods for the three structural systems

	LA	SE	BO
Fundamental Time Period	1.025502	1.341502	2.009776

Table 6-3 Capacity Spectrum analysis Results

Capacity Spectrum Method Results			
	Max Displacement (m)		
Earthquake	LA	SE	BO
Parkfield	0.1256	0.2799	0.3131
San Fernado	0.4337	0.4951	0.4196
Gazli USSR	0.018871	0.037949	0.10859
Bucharest	0.085086	0.2657	0.3479
TabasIran	0.03041	0.061154	US
Coyote Lake	0.1361	0.13045	0.11771
IMP E04	0.027214	0.054727	0.2248
IMP E05	0.03934	0.079112	US
IMP E06	0.04638	0.093268	US
IMP E07	0.041752	0.083962	US
IMP EMO	0.056753	0.12568	US

Table 6-4 Time History Results

Time History Results			
	Equivalent SDOF Max Displacement (m)		
Earthquake	LA	SE	BO
Parkfield	0.114953	0.214967	0.510619
San Fernado	0.380748	0.412918	0.378794
Gazli USSR	0.019029	0.036498	0.113061
Bucharest	0.078182	0.289596	0.335767
TabasIran	0.034724	0.062807	US
Coyote Lake	0.187957	0.163472	0.121013
IMP E04	0.026232	0.04863	0.269368
IMP E05	0.039465	0.079252	US
IMP E06	0.047938	0.095257	US
IMP E07	0.039023	0.079458	US
IMP EMO	0.050533	0.116395	US

$$\text{Percentage Error} = \frac{(U_{SDOF})_{Time\ History} - (U_{SDOF})_{Capacity\ Spectrum\ Method}}{(U_{SDOF})_{Time\ History}} \times 100$$

Table 6-5 Percentage Error

Percentage Error			
Earthquake	LA	SE	BO
Parkfield	-9	-30	39
San Fernado	-14	-20	-11
Gazli USSR	1	-4	4
Bucharest	-9	8	-4
TabasIran	12	3	US
Coyote Lake	28	20	3
IMP E04	-4	-13	17
IMP E05	0	0	US
IMP E06	3	2	US
IMP E07	-7	-6	US
IMP EMO	-12	-8	US

Table 6-6 Table Showing percentage error with the corresponding Pulse Period

	Percentage Error			
Earthquake	LA	SE	BO	T_p
Parkfield	-9	-30	39	2.00
San Fernado	-14	-20	-11	1.47
Gazli USSR	1	-4	4	4.20
Bucharest	-9	8	-4	2.13
TabasIran	12	3	US	5.26
Coyote Lake	28	20	3	1.00
IMP E04	-4	-13	17	4.44
IMP E05	0	0	US	3.92
IMP E06	3	2	US	3.85
IMP E07	-7	-6	US	3.64
IMP EMO	-12	-8	US	2.94

It can be observed that the percentage error (Table 6.6) for Parkfield, San Fernado and Coyote lake earthquakes are high. This can be explained looking at the pulse period for Boston building subjected to Parkfield earthquake pulse. The pulse period of this earthquake is 2.00 s which is the

same as the fundamental period of Boston building. Due to this the dynamic response is larger than static response. A similar behavior can be observed with Los Angeles and Seattle buildings subjected to Coyote lake acceleration pulse. Since the pulse period is almost equal to the fundamental period of LA and BO structures, it can be seen that the difference between results generated from nonlinear static analysis and dynamic time history analysis differ by a higher percentage of 28% and 20% respectively which can again be attributed to dynamic amplification. The capacity spectrum method fail to give good results for Seattle building subjected to Parkfield and San Fernado earthquake.

6.4 Conclusions

Capacity Spectrum method gives good results in most cases except for some cases where it does not converge. There are some other cases where dynamic amplification is observed when the fundamental period of the structure matches with the pulse period because of which in such cases the results of capacity spectrum method cannot be relied upon. The behavior of structures and applicability of the capacity spectrum method can be understood much better if the method is tested for more number of ground motion records and more number of structural systems.

REFERENCES

Mavroeidis GP, Papageorgiou AS. "*A mathematical representation of near-fault ground motions*". Bulletin of the Seismological Society of America 2003; 93:1099 –1131.

Mavroeidis GP, Papageorgiou AS. *"Near-fault ground motions, and the response of elastic and inelastic single-degree-of-freedom (SDOF) systems"*. Engineering & Structural Dynamics 2004; 33:1023–1049

Chopra, A. K. (2007). *"Dynamics of structures":* Theory and applications to earthquake engineering. Prentice-Hall, N.J.

Gupta A, Krawinkler H. "*Seismic demands for performance evaluation of steel moment resisting frame structures"* (SAC Task 5.4.3). Report No. 132, John A. Blume Earthquake Engineering Center, Stanford University, CA, 1999.

Gupta A, Krawinkler H. "*Estimation of seismic drift demands for frame structures"*. Earthquake Engineering & Structural Dynamics 2000; 29:1287–1305

Applied Technology Council _ATC_ 1997. *Seismic Evaluation and Retrofit of Concrete Buildings, prepared for the Seismic Safety Commission, State of California*, Report No. ATC-40 Redwood City, CA.

SeismoSoft [2007] SeismoStruct: *A computer program for static and dynamic nonlinear analysis* of framed structures (online), available from URL: http://www.seismosoft.com.

FEMA 351, 2000, *Recommended Seismic Evaluation and Upgrade Criteria for Existing Welded Moment Resisting Steel Structures,* prepared by the SEAOC, ATC, and CUREE Joint Venture for the Federal Emergency Management Agency, Washington, D.C.
(FEMA Publication No. 351).

ASCE, 2000, *Prestandard and Commentary for the Seismic Rehabilitation of Buildings*, FEMA 356 Report, prepared by the American Society of Civil Engineers for the Federal Emergency Management Agency, Washington, D.C.

Applied Technology Council _ATC_- 2005. *Improvement of nonlinear static seismic analysis procedures* FEMA 440 ,Report No. ATC-55 Redwood City, CA. prepared for Department of Homeland Security Federal Emergency Management Agency

Bernal, D. (1998). ‘‘*Instability of buildings during seismic response*.’’Engineering structures., 20(4–6), 496–502.

Challa, V. R. M., and Hall, J. F. (1994). ‘‘*Earthquake collapse analysis of steel frames*.’’ Earthquake Engineering and Structural Dynamics., 23(11), 1199–1218

MacRae, G. A. (1994). ‘‘*P-Delta effects on single-degree-of-freedom structures in earthquakes.*’’ Earthquake Spectra, 10(3).

Bernal, D. (1987). “*Amplification factors for inelastic dynamic p-delta effects in earthquake analysis*” Engineering & Structural Dynamics VOL 15:635-651 (1987)

.